Remote Sensing of Environment 134 (2013) 319–332

Contents lists available at SciVerse ScienceDirect

Remote Sensing of Environment

journal homepage: www.elsevier.com/locate/rse

Mapping biomass change after forest disturbance: Applying LiDAR footprint-derived models at key map scales

Wenli Huang [a,*], Guoqing Sun [a], Ralph Dubayah [a], Bruce Cook [b], Paul Montesano [a], Wenjian Ni [a,c], Zhiyu Zhang [c]

[a] Department of Geographical Sciences, University of Maryland, College Park, MD 20742, USA
[b] Biospheric Sciences Laboratory, NASA's Goddard Space Flight Center, Greenbelt, MD 20771, USA
[c] Institute of Remote Sensing Applications, Chinese Academy of Sciences, Beijing 100101, China

ARTICLE INFO

Article history:
Received 18 September 2012
Received in revised form 5 March 2013
Accepted 14 March 2013
Available online 12 April 2013

Keywords:
Above-ground biomass
Scale
Disturbance
Waveform LiDAR
LVIS

ABSTRACT

Accurate estimate of biomass and its changes at local to regional scales are important for a better understanding of ecosystem function, biodiversity and sustainability. In this study we explored the forest biomass prediction and dynamic monitoring from Light detection and ranging (LiDAR) waveform metrics at different key map scales. NASA's Laser Vegetation Imaging Sensor (LVIS) data were acquired in Penobscot County, Maine, USA, during August 2003 and 2009 airborne campaigns in the New England region. Field data were collected in 2003, and 2009 to 2011. Regression models developed at the scale of footprint were applied to all LVIS waveforms within the two study sites: Howland Forest (HF) and Penobscot Experiment Forest (PEF). The effect of forest disturbances on LVIS biomass prediction models was investigated. Two types of models, i. e. combined model without consideration of disturbances and disturbance-specific models were developed and compared. Field data from nested field plots of 0.25 ha, 0.5 ha and 1.0 ha were used to evaluate the averaged, footprint-level (~0.03 ha, 20 m diameter) estimates in these plots. The results demonstrate that: 1) prediction model at the scale of individual LVIS footprints is reliable when the geolocations of the measured footprints were determined by DGPS with a best accuracy of 0.5–1.0 m. 2) The differences between biomass prediction models for disturbed and undisturbed forests were statistically significant ($p < 0.001$) at the scale of footprint, and the disturbance-specific models performed slightly better ($R^2 = 0.89$, RMSE = 27.9 Mg·ha^{-1}, and relative error of 22.6%) than the combined model ($R^2 = 0.86$, RMSE = 31.0 Mg·ha^{-1}, 25.1%). 3) The evaluation using field plot data showed that the predictions of biomass were improved markedly with the increase of plot sizes from 0.25 ha to 1.0 ha and that the effect of disturbance was not strong. At 1.0 ha plot-level, both disturbance-specific and combined models agreed well with field estimates ($R^2 = 0.91$, 23.1 Mg·ha^{-1}, 16.1%; and $R^2 = 0.91$, 22.4 Mg·ha^{-1}, 15.6%). 4) Sensitivity analysis on levels of variation and error to footprint density suggests that a certain density of LVIS footprints is required for biomass mapping. The errors were minimized when footprint coverage approached about 50% of the area of 1.0 ha plots (16 footprints). 5) By applying the footprint-level models developed from 2009 LVIS data to both 2009 and 2003 LVIS data, the change of biomass from 2003 to 2009 could be assessed. The average annual biomass reduction rate from forest disturbance at two sites is −7.0 Mg·ha^{-1} and −6.2 Mg·ha^{-1}, the average annual biomass accumulation from regrowth is +4.4 Mg·ha^{-1} and +5.2 Mg·ha^{-1}, respectively.

1. Introduction

Above-ground biomass (here after biomass) stock from forest represents a significant component of the global carbon cycle (Goetz & Dubayah, 2011). Accurate estimate of forest biomass and its spatial distribution at fine resolution is required for a better understanding of terrestrial ecosystem function, biodiversity and sustainability (Bergen et al., 2009; Hall et al., 2011). Biomass can be estimated from field measurements based on well-defined allometric equations (Clark & Kellner, 2012). This traditional inventory method, which forms the basis for many national forest inventories, can be complemented and enhanced by the use of remote sensing techniques.

A variety of passive and active remote sensing techniques have been investigated for measuring and monitoring forest carbon stocks (Goetz & Dubayah, 2011; Lu, 2006). Light detection and ranging (LiDAR) is promising because of its ability to directly measure canopy vertical profile, providing canopy height information which is highly correlated with the forest biomass. LiDAR systems are categorized as small- or large-footprint based on the size of the illuminated ground

* Corresponding author. Tel.: +1 301 332 8859; fax: +1 301 314 9299.
E-mail address: wlhuang@umd.edu (W. Huang).

0034-4257/$ – see front matter © 2013 Elsevier Inc. All rights reserved.
http://dx.doi.org/10.1016/j.rse.2013.03.017

area. Small-footprint LiDAR systems (5–30 cm diameter) provide dense samples for detailed representation of the canopy structure, but their use is restricted to low-altitude airborne platforms. Small footprint full waveform systems have appeared in recent years with ability to record the complete waveform (Mallet & Bretar, 2009). Large-footprint laser systems (10–70 m diameter) record a continuous, vertical profile of returned signal. Although large-footprint LiDAR data is not able to capture the very fine spatial details of forest canopies, structural attributes can be derived from vertical profiles of return energy for application in ecology studies (Mather, 2004). LiDAR derived metrics from small-footprint discrete return LiDAR (Asner et al., 2010; Gonzalez et al., 2010; Lim & Treitz, 2004; Næsset & Gobakken, 2008; Nilsson, 1996; Pang et al., 2008; Zhao et al., 2011) and continuous returned full-waveform LiDAR (Drake et al., 2002, 2003; Dubayah et al., 2010; Lefsky, 2010; Lefsky et al., 1999, 2002, 2005a, 2007; Means et al., 1999; Ni-Meister et al., 2010; Sun et al., 2008) have been used for estimation of forest canopy height and biomass. Various multi-sensor fusion (Asner et al., 2010, 2012; Kellndorfer et al., 2010; Lefsky et al., 2005b; Nelson et al., 2009; Saatchi et al., 2011; Sun et al., 2011; Swatantran et al., 2011) used LiDAR samples and optical or radar imagery data for regional to continental mapping of forest attributes.

Laser Vegetation Imaging Sensor (LVIS) (Blair et al., 1999) with a footprint size of 10–25 m, records the entire profile (waveform) of the return signal in ~30 cm vertical bins (Dubayah et al., 2000). Because the footprint size is larger than the diameter of a tree crown and the laser beam can pass gaps between trees, a waveform can capture the tree top and ground surface in a forest stand. Studies have confirmed the ability of LVIS-derived metrics to estimate biomass, even in dense tropical forests. Drake et al. (2002) reported that height of mean energy (HOME or RH50) is the best single term predictor for estimating tropical forest biomass at the LVIS footprint-level (~0.05 ha, 25 m diameter) and the plot-level (~0.5 ha). The issue of sampling sizes has also been discussed by several studies with small- to large-footprint LiDAR system. Drake et al. (2002) compared regression models at the footprint-level and the plot-level for a tropical wet forest at La Selva, Costa Rica. They found that because of geolocation uncertainties, large tree location, and species composition, the prediction model was better at plot-level with the R^2 of 0.73 and RMSE of 60.02 $Mg \cdot ha^{-1}$. Results from Hyde et al. (2005) indicated a strong agreement between field data and LVIS measurements for height ($R^2 = 0.75$; RMSD = 8.2 m) and biomass ($R^2 = 0.83$; RMSD = 73.5 $Mg \cdot ha^{-1}$) at Sierra Nevada sites in California, but not for canopy cover. Anderson et al. (2006) found good relationship between LVIS metrics and height ($R^2 = 0.80$), but the relationship is weaker between metrics and biomass ($R^2 = 0.61$, RMSE = 58 $Mg \cdot ha^{-1}$) at Bartlett Experimental Forest (BEF) in New Hampshire, USA. According to Anderson et al. (2008), the possible factors for a weaker correlation include geolocation error, species composition, and intensity of disturbance. Dubayah et al. (2010) applied the LVIS data for mapping biomass change. They found various issues that need to be considered in detecting and mapping the biomass change with LVIS data, and suggested using range-distance based ΔRH_E metrics to develop the uniform biomass change equation at plot-level to avoid errors caused by ground detection and two sets of regression models. Asner et al. (2010) noted the scaling issue that the small-footprint LiDAR prediction errors decrease with the increase of plot size. Mascaro et al. (2011) proposed a "crown-distributed" approach to address the plot and edge scaling issues caused by the disagreement between LiDAR and field measurements.

The effects of disturbance on the relationship between biomass and height metrics were investigated by field observations and model simulation. Drake et al. (2003) investigated the relationships of simple LiDAR metrics (i.e. RH50) with estimated biomass, and indicated that there are significant differences between different types of forest (i.e. tropical wet forest and tropical moist forest). Ni-Meister et al. (2010) indicated that combined height and gap fraction could improve the estimation of biomass particularly for coniferous. Ranson and Sun (2010) simulated the waveform RH metrics from different stands (disturbed and undisturbed forest) by a 3D-LiDAR model, and showed that the relationships between forest biomass and LiDAR metrics were distinguishable. Asner et al. (2011) found that the fitted curves between forest carbon stocks and LiDAR signals are different from plantations and natural regrowth after disturbance because of stocking differences. Inventory data and modeling results also demonstrated that young forests accumulated biomass much faster than the matured forest for the first 10 to 20 years after disturbance (Chazdon, 2003). Vegetation change tracker (VCT) algorithm was designed for detecting forest disturbance (Huang et al., 2010) via spectral–temporal information from Landsat time series stack (LTSS). The products of yearly disturbance maps from LTSS-VCT were used in this study.

The biomass prediction models can be developed at the scale of footprints and larger plots. To facilitate regional and global biomass mapping using LiDAR waveform data, models at footprint-level are desirable because sampling large plots is much more time consuming than footprint-level sampling. The accuracy of biomass estimation at coarser scales will depend on the accuracy of the footprint-level models and the number of samples (footprints) at this scale. In this study we will investigate 1) if the model at footprint-level can be developed with desirable accuracy in our study sites, 2) if the forest management practices in terms of disturbances will affect the models, and 3) what will be the proper scale with concern of uncertainties for mapping biomass from LVIS data in our study sites. Forest biomass map at 1.0 ha pixel size was produced from LVIS acquired in 2003 and 2009. The changes of biomass from 2003 to 2009 were analyzed in this study.

2. Study area and data acquisition

The study sites are located in Penobscot County, Maine, USA (Fig. 1). These include Howland Forest (HF) in the Northern Experimental Forest (45°08′–45°14′ N, 68°42′–68°45′ W), and the Penobscot Experimental Forest (PEF) (45°49′–45°52.5′ N, 68°30′–68°38.5′ W). Both sites consist of boreal forest with mixed deciduous and coniferous tree species (Hollinger et al., 1999; Safford et al., 1969). The dominant species include *Populus tremuloides* (quaking aspen), *Betula papyrifera* (paper birch), *Tsuga canadensis* (eastern hemlock), *Picea rubens* (red spruce), *Abies balsamea* (balsam fir), and *Acer rubrum* (red maple). The region features relatively level and gently rolling topography. According to USGS 1/3-Arc Second National Elevation Dataset (NED) published in 2009, the elevation ranges from 40 m to 178 m at HF, and from 29 m to 83 m at PEF. HF has an American Flux Tower within intermediate aged forest, and the surrounding areas are private land owned by a timber production company with different forest management manipulations such as clear-cut, select-cut and stripe-cut.

2.1. Field campaign

Field measurements were conducted during August 2009 to 2011. Both footprint-level (~0.03 ha, 20 m diameter) and plot-level (0.25 ha–1.0 ha) plots (see Fig. 2 for typical layout) were measured. Differential Global Position System (DGPS) instruments were used to locate LVIS footprints and establish sampling plots.

At the plot-level, twenty-four 1.0 ha (200 m × 50 m) plots and ten 0.5 ha (100 m × 50 m) plots were established in 2009 and 2010, respectively. The longer edges of these plots were in the range direction of the NASA/JPL Uninhabited Aerial Vehicle Synthetic Aperture Radar (UAVSAR) flight lines. The layout of these plots is illustrated in Fig. 2, where each plot consists of sixteen 25 m × 25 m subplots.

At the footprint-level, ninety-one circular plots with 20 m diameter centered at each LVIS footprint were selected in both undisturbed forest and disturbed forest. Forty-seven footprints were measured in August, 2010 and forty-four were measured during January and August of 2011.

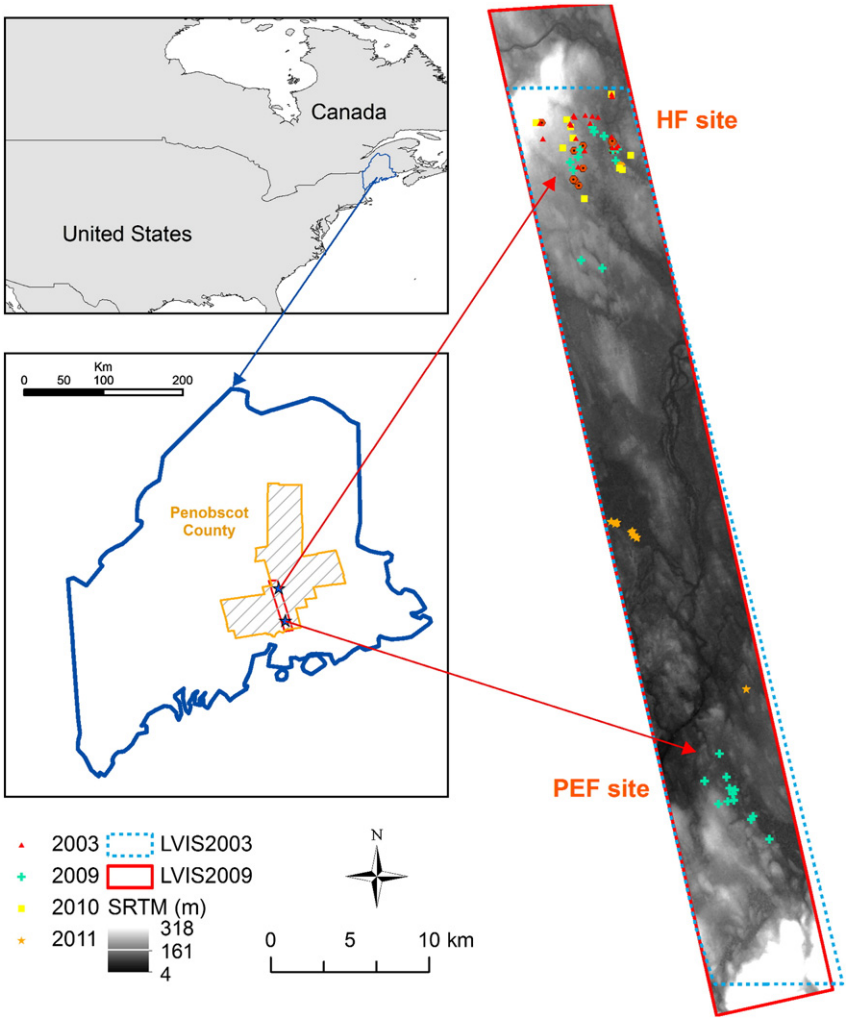

Fig. 1. Location of study area and field sites: the site in north is Howland Forest (HF), and the site in south is Penobscot Experimental Forest (PEF).

Diameter at Breast Height (DBH, diameter at 1.3 m above ground), species for ever tree with DBH ≥ 10 cm, top height, height of crown base and crown width of the three highest trees in each subplot were recorded. A census of stems below the established size threshold (DBH < 10 cm) and height ≥1.3 m were sampled within a 2 m transect along the center of the rectangular plot, and from north-to-south in footprint-level circular plots. The number of stems falling into four diameter categories (i.e. 0–2 cm; 2–5 cm, 5–8 cm and 8–10 cm) was counted and used as a representative sample of all small stems in the plot.

Collections of field data during the October 2003 campaign were described by Sun et al. (2011). Seventeen forest inventory samples within the HF study site were used for the evaluation of 2003 biomass map. For each inventory sample, three to four plots with radius of 4 m, 7 m or 10 m were arranged in the center, 30 m north, south-west, and south-east from the center. The DBH for every tree with a DBH > 3 cm, and the height, crown length and width of 8 trees in each plot were measured.

2.2. LiDAR data

The Laser Vegetation Imaging Sensor (LVIS) is a large footprint airborne scanning laser altimeter developed by NASA Goddard Space Flight Center (GSFC) (Blair et al., 1999, 2006). LVIS data of study area were acquired during leaf-on season in July of 2003 and August of 2009. For both

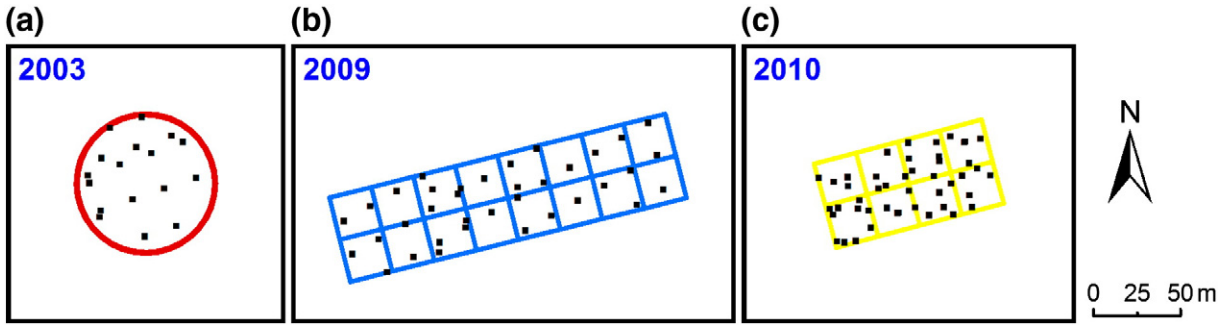

Fig. 2. Layout of typical field plot in 2003, 2009, and 2010: (a) stand plot (80 diameter) in 2003; (b) 1.0 ha (50 m × 200 m) plot in 2009; (c) 0.5 ha (50 m × 100 m) plot in 2010. Black dots are LVIS footprint center.

years, the footprints had a nominal diameter of 20 m. The 2003 data was reprocessed in 2008, thus it is more consistent with the 2009 data.

LVIS products of version 1.02 provide three types of datasets: LVIS Canopy Elevation (LCE), LVIS Geolocated Elevation (LGE), and LVIS Ground Waveforms (LGW) (Blair et al., 2006). From the waveform, mean elevation of the lowest detected mode is defined as ground elevation (zg). Then, relative heights (RH) to the ground elevation are calculated at quartile percentage of cumulative waveform energy (i.e., 25%, 50%, 75%, and 100%). The footprint density varies at different locations in the study area because of overlapping flight lines during the campaign.

2.3. Auxiliary data

LTSS-VCT disturbance products were used in this study to identify disturbed forests from undisturbed ones (Huang et al., 2010). The study area is located in the center of Landsat p011/r029 of the World Reference System (WRS) with good quality images. Subset product maps are used in this study to differentiate the year of disturbances. The product detects most of clear-cut events, however, it has missed some stripe-cuts around 1990–1995 and select-cut (shelterwood harvest) after 2000 at HF site. Similar problem has been noticed and documented at other validation sites in USA (Thomas et al., 2011). Therefore, a further forest management map was created from operation information from the private owner (International Paper®, IP Company) and Google images at HF site. Several patches of disturbed forest were digitized from Google Earth images and combined with digitized version of management operation maps in different year. These maps were used to identify the occurrence of disturbance, and will be explained in details in sections of Results and Discussion.

3. Methodology

3.1. Allometric-based biomass calculation

The diameter-based allometric equations used for large stems (DBH ≥ 10 cm) and small stems (DBH < 10 cm) came from the comprehensive report of USDA on North American forest (Jenkins et al., 2003, 2004). Biomass of large stems was calculated by corresponding species-specific allometric equations. Biomass of the small stems was calculated by mixed hardwood equations using the midpoint of the diameter class (i.e., 1.0 cm, 2.5 cm, 6.5 cm and 9.0 cm) as the DBH times the number of stems in each category. Biomass was first calculated for each stem, and then total biomass was aggregated from subplot to plot levels.

3.2. LiDAR data processing

Relative height metrics (RH25, RH50, RH75 and RH100) of LVIS waveform were retrieved from LVIS LGE datasets for all sampling plots and measured footprints. The LVIS RH metrics of the study sites (HF and PEF) in 2009 were shown in Fig. 3 as false color images (R: RH50, G: RH100, B: RH25). Images were created by interpolating of point data into 15 m grid with a Delaunay triangulation method (TRIGRID function) provided by IDL version 7.1 (Exelis, Boulder, CO).

The change of canopy profiles in waveform reveals the biomass change between 2003 and 2009. Waveforms acquired in 2003 and 2009 at HF site are shown in Fig. 4. The distances between the waveform centers in 2003 and 2009 were less than 2 m. These waveforms represent the disturbed forest with (a) near-mature forest with neutral changes, (b) disturbed forest with negative change of RH metrics, and (c) forest with positive change of RH metrics, respectively.

The density of LVIS waveforms in each field plot varied depending on number of overlapping flight lines at a given portion of forest. The nominal spacing of LVIS footprint is 20 m both along and cross track. Ideally, the nominal footprint density within a plot would be 9, 18, and 36 at sizes of 0.25 ha (50 m × 50 m), 0.5 ha (50 m × 100 m) to 1.0 ha (50 m × 200 m). However, two factors lead to a varied footprint density. First, there were overlapping LVIS flight lines for our study site. Similar issues have been mentioned at other LVIS study sites such as Sierra site in California (Hyde et al., 2005), Bartlett site in New Hampshire (Anderson et al., 2008), and La Selva site in Costa Rica (Dubayah et al., 2010). In addition, the long edges of 50 m × 200 m field plots were set along the range direction of the UAVSAR data, which has a 10–20° angle to the LVIS's flight direction as shown in Fig. 2(b)–(c). Therefore, the averaged footprint density within the measured plots in 2009 and 2010 was not consistent and

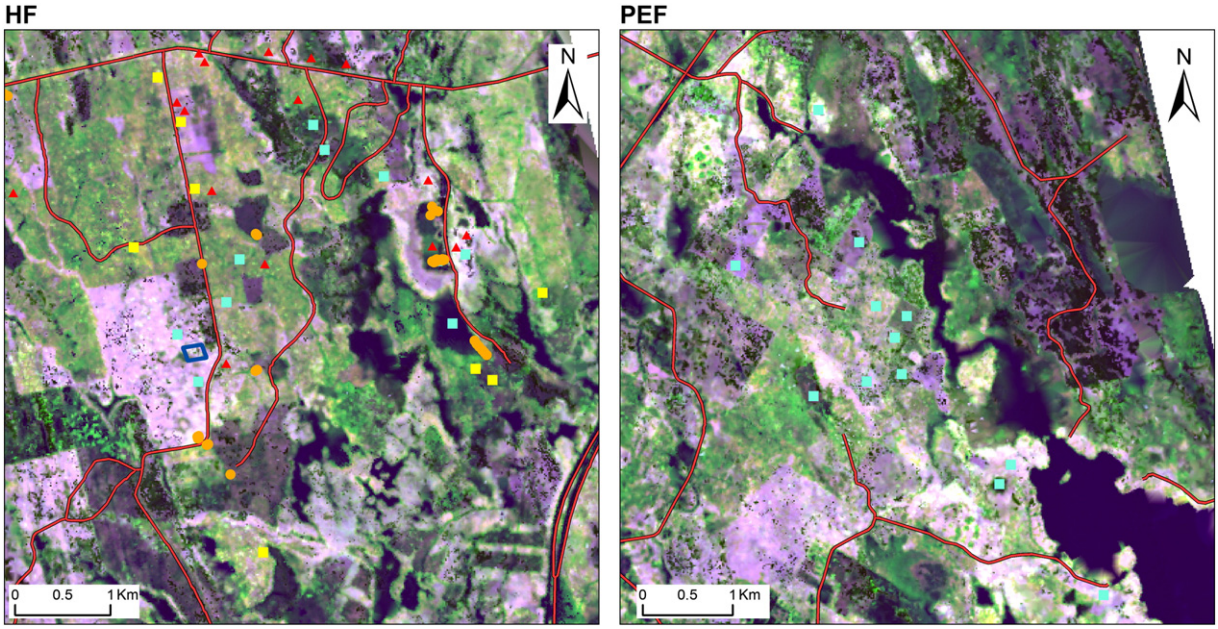

Fig. 3. Images of gridded RH (R: RH50, G: RH100, B: RH25) metrics over study sites in 2009: Left — HF; right — PEF. Red lines are major roads. Dark blue rectangle in HF is the stem-map site. Field measurements are labeled with different colors for 2003 (red), 2009 (cyan), 2010 (yellow) and 2011 (orange).

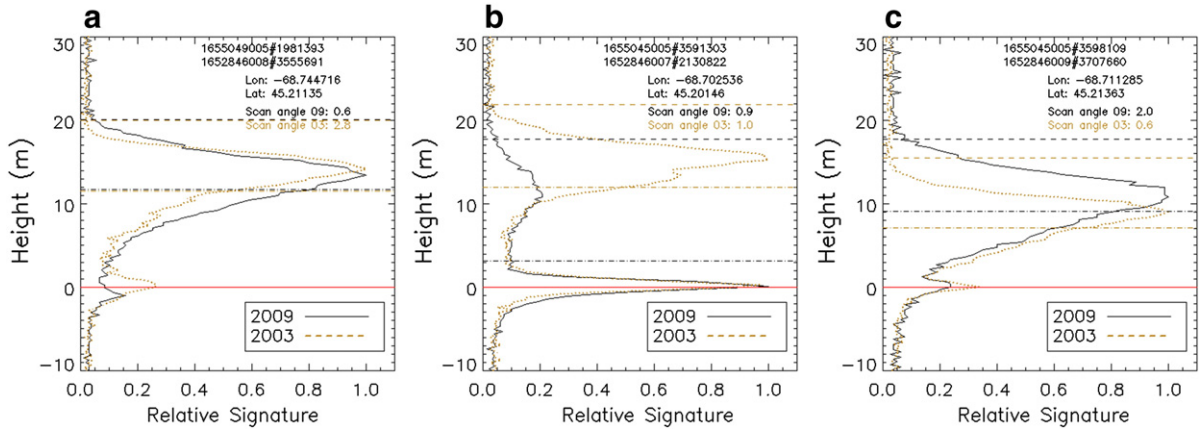

Fig. 4. Typical co-incident waveforms (center within 2 m) from LVIS 2003 and 2009 data: Black solid waveform is from 2009, gold dash waveform is from 2003. Red solid line is the detected ground in LGE, dashed straight lines are the RH100, dashed with dot lines are the RH50. (a) RHs relatively unchanged; (b) RHs have significant negative changes; (c) RHs with positive change.

varied from 14, 27, and 53 footprints per plot from 0.25 ha, 0.5 ha to 1.0 ha plot-levels.

While processing the footprint-level field samples, two samples in the near matured old-growth forest region were found with wrong ground elevation (zg from LVIS LGE product) values. This discrepancy has been mentioned in LVIS known data set issues (http://lvis.gsfc.nasa.gov/DataDisclaimer.html), which is caused by insufficient energy returned from the ground and errors associated with the automated peak-finding algorithm. These two points were corrected in this study by finding a mean ground elevation of their neighboring footprints.

3.3. Forest disturbance identification

All sampled plots were classified as undisturbed or disturbed based on LTSS-VCT yearly disturbance product (1984 to 2010), high-resolution images and field notes. Forest disturbance maps were generated to show the disturbances prior to 2003, during 2003 to 2009 and after 2009 using the abovementioned data and forest management information from the owner. Most of the disturbed plots in HF site were those disturbed by management activities (Sun et al., 2011), including clear-cut stands in the 1980s, stripe-cuts in the 1990s and select-cuts (shelter-wood harvest) after 2000. A few tree plantations in our study site were also labeled as disturbed forest, as they were mainly planted after clear-cut. While the disturbance data we used relied heavily on the LTSS-VCT, we enhanced the classification using visual interpretation of high resolution imagery and field notes to refine the boundaries of forest disturbance patches. In addition, National Land Cover Data (NLCD) products in 2001 and 2006 were used to discriminate forest and non-forest for the entire study area. Woody forestlands and wetlands were included as forests in our analysis.

The sampled footprints consist of 47 undisturbed (51.6%) and 44 disturbed (48.4%) samples. The mean biomass value of undisturbed field samples (157.1 $Mg \cdot ha^{-1}$) was higher than that of disturbed ones (87.4 $Mg \cdot ha^{-1}$). At 0.25 ha plot-level, there were 41 undisturbed and 64 disturbed plots. At 0.5 ha plot-level, there were 18 undisturbed and 34 disturbed plots. At 1.0 ha plot-level, there were 10 undisturbed and 12 disturbed plots.

3.4. Mapping forest biomass and changes

The mapping procedure consists of four steps: 1) develop the biomass estimation models from 2009 LVIS waveform data at the footprint-level and choose the best one; 2) evaluate the model performance with the plot-level observation data in 2009 and 2003, and determine the pixel size of the biomass map to be generated; 3) apply the selected model to generate biomass maps in both 2009 and 2003 with LVIS waveform data; and 4) detect the change in biomass from 2003 to 2009. The first two steps are shown in a conceptual workflow in Fig. 5.

This study employed several widely used statistical indicators to evaluate the accuracy of different regression models. Indicators included squared coefficient of determination (R^2), root mean square error (RMSE), and RMSE (%) which is the ratio of RMSE to mean observed value:

$$\mathrm{RMSE}(\%) = \frac{\mathrm{RMSE}}{\overline{y}} \quad (1)$$

where $\overline{y}$ is the mean biomass.

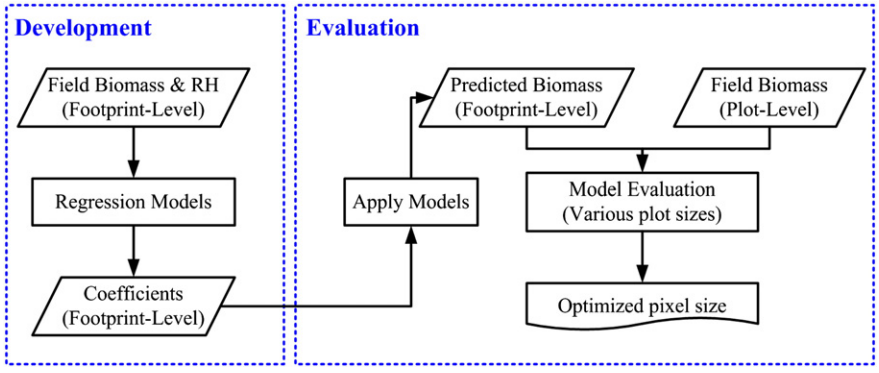

Fig. 5. Workflow of model development and evaluation for biomass mapping.

Table 1
Correlation between RH metrics of LVIS footprint samples.

	RH25	RH50	RH75	RH100
RH25	1.00			
RH50	0.90	1.00		
RH75	0.79	0.96	1.00	
RH100	0.72	0.87	0.95	1.00

3.4.1. Development of regression models

Linear regression models were developed relating field-measured biomass and LVIS metrics at footprint-level and evaluated at different plot-level (i.e. 0.25 ha, 0.5 ha and 1.0 ha rectangular plot). Two types of models were developed, i.e. combined model without consideration of disturbances and disturbance-specific models.

RHs metrics are highly correlated as shown in Table 1, so we only develop the single term regression models.

A dummy variable was introduced into the linear regression model to test the effect of disturbances on intercepts and slopes (Solberg et al., 2010). This dummy variable is used to indicate the occurrence of disturbance, where the truth is represented by a numerical value of 1. Then the equation becomes:

$$\text{Biomass} = \beta_1 + \beta_2 X_1 + \beta_3 X_2 + \beta_4 X_1 X_2 + e_i \quad (2)$$

where β_1–β_4 are estimated parameters, X_1 is the RH metrics in meters, X_2 is the dummy variable with values 0 (undisturbed) or 1 (disturbed), and e_i is the error item. The hypothesis is H_0: $B_{undisturbd} - B_{disturbed} = 0$ or $\beta_4 = 0$. If $\beta_4 = 0$ then we will reject the H_0 which means that the undisturbed and disturbed models are the same, otherwise they are different.

3.4.2. Evaluation of prediction models by field biomass data

Biomass of LVIS footprints within field plots was predicted from the footprint-level model and aggregated to the plot-levels. Then it was compared with corresponding field measurement. For 2009 data, the predicted biomass was evaluated with field measurements aggregated at three scales of plot-levels: 0.25 ha, 0.5 ha and 1.0 ha. For 2003 data, the field biomass was measured with FIA-style field measurements at ~0.5 ha plot-level. The predicted biomass was an average of the biomass from the footprints within a circle of 80 m diameter. The best mapping pixel size was determined by the plot-level model evaluation. Generally the aggregation footprint-level samples to larger plots reduced the overall variance and impact of geolocation errors (Hall et al., 2011). Two studies (Frazer et al., 2011; Mascaro et al., 2011) have recently shown similar pattern that LiDAR prediction errors reduced at larger plot sizes. The optimized pixel size for biomass mapping was selected based on statistical measurements including averaged prediction value, R^2, RMSE, and bias.

3.4.3. Biomass mapping from LVIS data

The mapping procedure is illustrated in Fig. 6. First, two masks were created. A persistent non-forest mask was generated from NLCD product in 2001 and 2006. Non-forest pixels in both years were excluded from the mapping in this study. In addition, a data

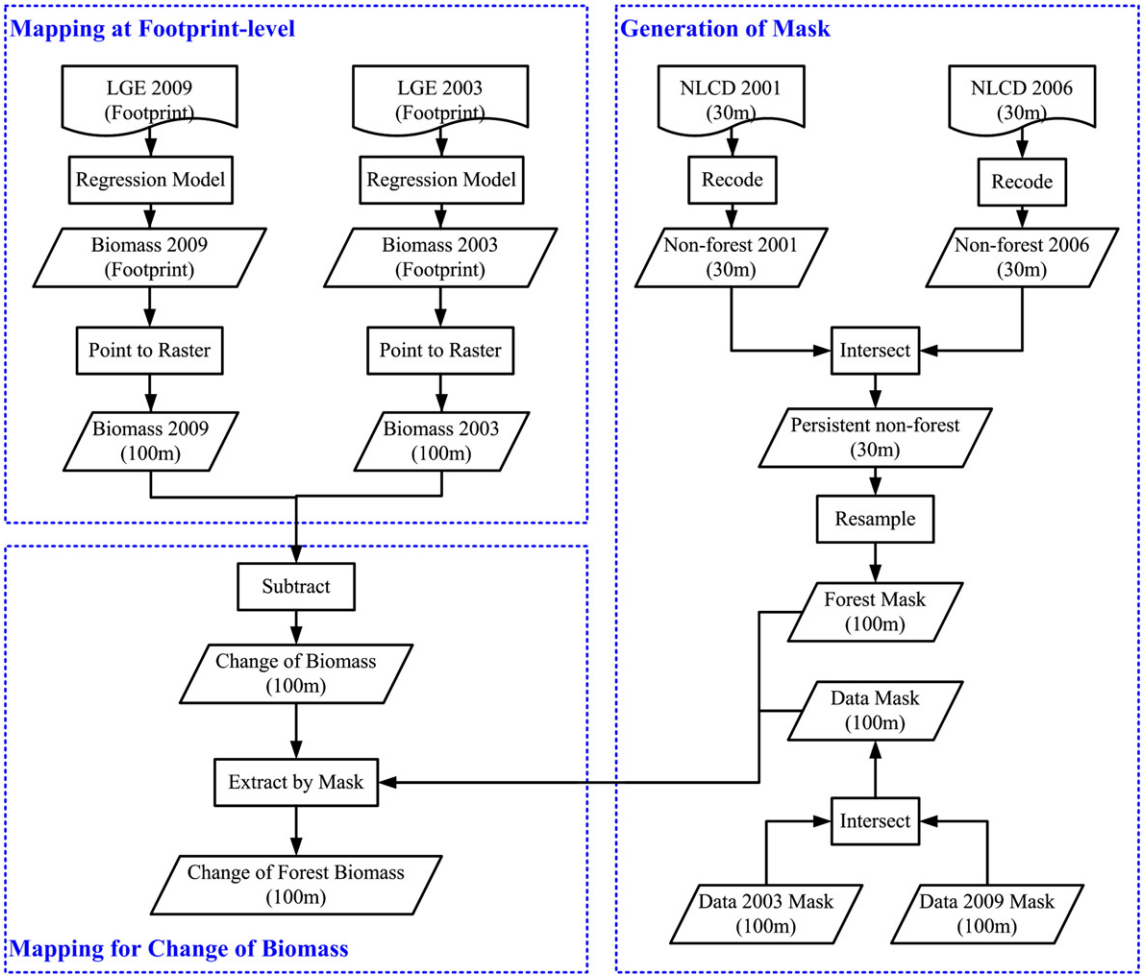

Fig. 6. Biomass mapping and change detection from LVIS data.

Table 2
Summary of single term regression models at footprint-level for 2009 data.

Model (ft-level)	Intercept	Slope	R^2	RMSE ($Mg \cdot ha^{-1}$)	RMSE (%)
Bio-RH25	90.8	22.0	0.70	45.1	36.5
Bio-RH50	**30.3**	**16.1**	**0.86**	**31.0**	**25.1**
Bio-RH75	−3.3	13.5	0.84	33.0	26.6
Bio-RH100	−51.9	11.1	0.74	42.1	34.2

Number of samples: 91; Mean of field measurements is 123.4 $Mg \cdot ha^{-1}$; Bolded data are the selected model.

coverage mask was created for the area common to both LVIS data in 2003 and 2009. These masks were gridded into the selected optimized pixel size to match the biomass mapping scale. Next, the regression model was applied to the LVIS footprints of entire study area in 2003 and 2009. Finally, the mean value of the footprint-level biomass within each grid cell was calculated and assigned to the pixel. The biomass change map was generated by subtracting 2003 biomass from that in 2009 within the forested area common to both LVIS data collections.

4. Results

4.1. Model performance at the LVIS footprint-level

4.1.1. Single term regression model

Table 2 shows the biomass prediction from single term regression models. The biomass models at the footprint-level by all four RH metrics have high R^2 values ranging from 0.70 to 0.86. For all groups, there were strong and significant correlations ($p < 0.005$) between biomass and RH metrics. The RH50 and RH75 metrics perform similarly in terms of R^2, RMSE and RMSE (%). Averaged field biomass of 91 sampled footprints was 123.4 $Mg \cdot ha^{-1}$. As mentioned above RH metrics are highly correlated. The correlation is as high as 0.96 between RH75 and RH50. Therefore, the single term regression model using RH50 was selected for the combined prediction model at the footprint-level for all data as it explains the greatest proportion of variance ($R^2 = 0.86$), and has the lowest residual error (RMSE = 31.0 $Mg \cdot ha^{-1}$, and a relative error 25.1%).

Fig. 7 shows the relationship between field biomass and RH50 and the contrast between undisturbed and disturbed groups at footprint-level. From Fig. 7(b), we could visually observe the two groups with different slopes of their trend lines. A statistical measurement (described in Section 3.4.1) was used to test the disturbance effect on intercepts and slopes in the next section.

4.1.2. Disturbance effect test

Following equation is from the regression when a dummy variable "disturb" with value 0 for disturbed and 1 for undisturbed forest was added for RH50 model:

$$Bio = 33.2 + 16.9 * RH50 - 3.7 * disturb - 4.6 * RH50 * disturb \quad (3)$$

with Multiple R^2: 0.94, standard error: 28.7 $Mg \cdot ha^{-1}$, F-statistic: 224.7 on 3 and 87 degrees of freedom, and a $p < 0.001$.

Since the coefficient for the dummy variable ($\beta_4 = -4.6$) is not equal to zero, we reject the H_0 hypothesis. The effect of disturbances on biomass estimation model from RH50 is significant.

The dummy variable was also added to RH75 model and the regression equation was:

$$Bio = -8.6 + 15.4 * RH75 - 22.7 * disturb - 6.0 * RH75 * disturb \quad (4)$$

with Multiple R^2: 0.95, standard error: 24.7 $Mg \cdot ha^{-1}$, F-statistic: 309.3 on 3 and 87 degrees of freedom, and a $p < 0.001$.

Hence, we also rejected the H_0 hypothesis for the RH75 model.

A student T-test with two tails, unequal sample sizes, and unequal variance was employed to measure the disturbance effect on the predicted biomass. The T-test showed that disturbance has a significant effect on the predicted biomass from both RH50 ($p < 0.001$) model and RH75 ($p < 0.001$) model.

Thus, footprint-level single term models were developed for undisturbed and disturbed forest with RH50 and RH75 models. As shown in Table 3, both the RMSE and RMSE (%) were reduced for the disturbance-specific RH50 and RH75 models. Even though the R^2 and RMSE of the disturbance-specific models were not always better than the combined model, the comparisons between the field biomass and predicted biomass of all sample footprints showed better results from disturbance-specific models. The third lines in RH50 and RH75 of the disturbance-specific models are the results of comparing predicted biomass with field biomass of all sampling footprints. Disturbance-specific models explained higher predicted variance (RH50, $R^2 = 0.89$; RH75, $R^2 = 0.91$) than the combined model (RH50, $R^2 = 0.86$; RH75, $R^2 = 0.84$). RMSE (RH50, 27.9 from

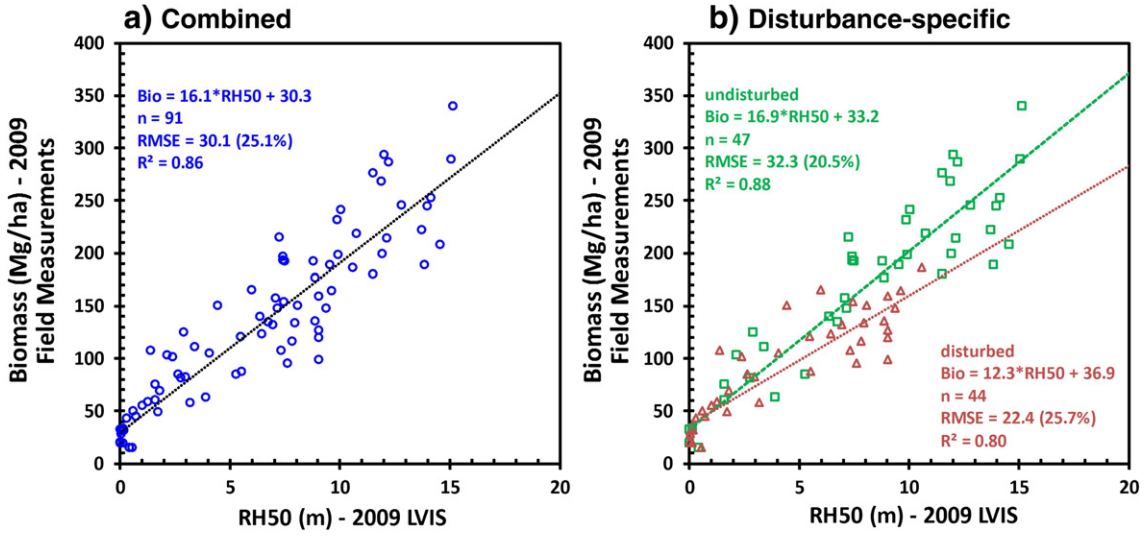

Fig. 7. Relationship between field biomass and LVIS relative height metric RH50 at footprint-level: (a) Combined model; (b) Disturbance-specific models. Different colors indicate different models: rectangle dots (green) represent the undisturbed group, and triangle dots (red) represent the disturbed group.

Table 3
Combined and disturbance-specific models at footprint-level.

Model	Variable	N	GP#	Intercept	Slope	R^2	RMSE ($Mg \cdot ha^{-1}$)	RMSE (%)
Combined	**RH50**	**91**	**all**	**30.3**	**16.1**	**0.86***	**31.0**	**25.1**
	RH75	91	all	−3.3	13.5	0.84*	32.9	26.6
Disturbance-specific	RH50	47	1	33.2	16.9	0.88*	32.3	20.5
		44	2	36.9	12.3	0.80*	22.4	25.7
		91	all	–	–	0.89*	27.9	22.6
	RH75	47	1	−8.6	15.4	0.89*	30.0	19.1
		44	2	14.1	9.4	0.90*	15.9	18.2
		91	**all**	–	–	**0.91***	**24.2**	**19.6**

GP#: 1 is undisturbed plot group, 2 is disturbed plot group; N: number of sample; Bolded data are models with best performance by evaluation at corresponding scale.
* p-value < 0.005.

31.0 $Mg \cdot ha^{-1}$; RH75, 24.2 from 32.9 $Mg \cdot ha^{-1}$) as well as RMSE (%) (RH50, 22.6% from 25.1%; RH75, 19.6% from 26.6%) were reduced. The large differences in RMSE (%) for different groups (disturbed, undisturbed and all) are partially caused by the differences of mean biomass. The mean biomass of the undisturbed forest (157.1 $Mg \cdot ha^{-1}$) is over 50% larger than that of the disturbed (87.4 $Mg \cdot ha^{-1}$), and also larger than that of the combined plots (123.4 $Mg \cdot ha^{-1}$).

4.2. Evaluation of prediction model

4.2.1. Evaluation of combined prediction model in 2009 and 2003

The footprint-level RH50 model from the combined data (Bio = 30.3 + 16.1 * RH50) was applied to 2009 LVIS data and evaluated at three plot-levels: 1) 0.25 ha plot (50 m × 50 m), 2) 0.5 ha plot (50 m × 100 m), and 3) 1.0 ha plot (50 m × 200 m), respectively. The evaluation plots were also divided into disturbed and undisturbed plots using LTSS-VCT and Google Earth images.

Evaluation of the combined footprint-level models with plot-level field data was shown in Table 4. As expected, the best model at three plot-levels in 2009 is RH50 model with higher explanation of total variance, lower RMSE and lower bias. The overall model performance improved with larger plot size from 0.25 ha, 0.5 ha to 1.0 ha. At 1.0 ha plot-level, the combined RH50 model explained 91% of the total variance with a positive bias of 2.0 $Mg \cdot ha^{-1}$ (1.4%) and RMSE of 22.4 $Mg \cdot ha^{-1}$·(15.6%).

Fig. 8 shows the scatter plot of predictions versus field measurements from the best combined footprint-level prediction model. In 2009, the combined RH50 model has better performance than RH75 model from evaluations at all three plot-levels. While in 2003, the combined RH75 model was better than combined RH50 model. There is almost no bias (less than ±1.3%) observed for predictions in 2009, but the evaluation of 2003 biomass prediction at sampling sites showed worse results. In 2003, the combined RH75 prediction model overestimates the biomass with a positive bias of 11.9 $Mg \cdot ha^{-1}$ (+7.9%). It has lower explanation of total variance (54%) and higher RMSE of 46.6 $Mg \cdot ha^{-1}$. The combined RH50 model also overestimates the biomass and has similar explanation of total variance (53%) and higher RMSE. A part of the reason is that the plot size and shape in 2003 (80 m diameter circle, ~0.5 ha) were different from 2009 (rectangular) which leads to an inconsistency. The number of sample in 2003 is relatively small compared with that of 0.5 ha plot-level samples in 2009. In addition, the GPS unit used in 2003 for field-sampled plot wasn't as good as the one for 2009, which leads to geolocation errors.

4.2.2. Evaluation of disturbance-specific prediction models in 2003 and 2009

Similar steps were conducted to evaluate the disturbance-specific models by different plot-level data. Evaluation results were shown in Table 5. It can be seen from comparing the R^2 listed in Tables 4 and 5 that the disturbance-specific models preformed slightly better than common models. The disturbance-specific RH50 model has almost the same values of explanation of variance and RMSE as the combined RH50 model. At 1.0 ha plot-level, the disturbance-specific RH50 model explained 91% of the total variance, with a positive bias of 0.9 $Mg \cdot ha^{-1}$ (0.6%) and RMSE of 23.1 $Mg \cdot ha^{-1}$ (16.1%). The bias was reduced from −3.0 $Mg \cdot ha^{-1}$ to 0.9 $Mg \cdot ha^{-1}$ from 0.25 ha to 1.0 ha plot-levels.

Fig. 9 shows the scatter plots of predictions versus field measurements from the best disturbance-specific footprint-level models at various plot sizes. The RH50 model has the best performance at all plot levels and in both 2009 and 2003. Again, there is almost no bias (less than ±2.0%) observed for predictions in 2009 and a less than +13.5% bias in 2003. Similar to the combined RH models, the disturbance-specific models overestimated the biomass for 2003.

Even though the statistical tests of prediction models at footprint level showed significant effect of disturbance, the evaluation of the predicted biomass demonstrated that the disturbance effect is reduced in a larger sampling area. For further biomass mapping and change detection the combined RH50 model was used and the biomass maps were generated at 1.0 ha (100 m × 100 m) spatial resolution.

Table 4
Evaluation of the footprint-level combined RH50 and RH75 models by plot-level field data in 2009 and 2003.

Model	Year	Plot-size	N	Mean of field ($Mg \cdot ha^{-1}$)	Mean of predict ($Mg \cdot ha^{-1}$)	R^2	RMSE ($Mg \cdot ha^{-1}$)	RMSE (%)	Bias ($Mg \cdot ha^{-1}$)	Bias (%)
RH50	**2009**	**0.25 ha**	**105**	**143.6**	**144.5**	**0.79**	**32.6**	**22.7**	**+0.8**	**+0.6**
		0.5 ha	**52**	**142.7**	**144.4**	**0.83**	**28.5**	**20.0**	**+2.2**	**+1.5**
		1.0 ha	**22**	**143.8**	**145.8**	**0.91**	**22.4**	**15.6**	**+2.0**	**+1.4**
	2003	0.5 ha	17	151.0	168.0	0.53	50.4	33.4	+17.0	+11.2
RH75	2009	0.25 ha	105	143.6	147.1	0.72	37.3	26.0	+3.5	+2.4
		0.5 ha	52	142.7	147.7	0.76	33.8	23.7	+4.9	+3.5
		1.0 ha	22	143.8	144.6	0.84	28.5	19.8	+0.8	+0.5
	2003	**0.5 ha**	**17**	**151.0**	**162.9**	**0.54**	**46.6**	**30.9**	**+11.9**	**+7.9**

N: number of sample; Mean of field: mean biomass averaged over samples at plot-level; Mean of predict: mean predicted biomass averaged over samples at plot-level; Bolded data are models with best performance at corresponding scale and year.

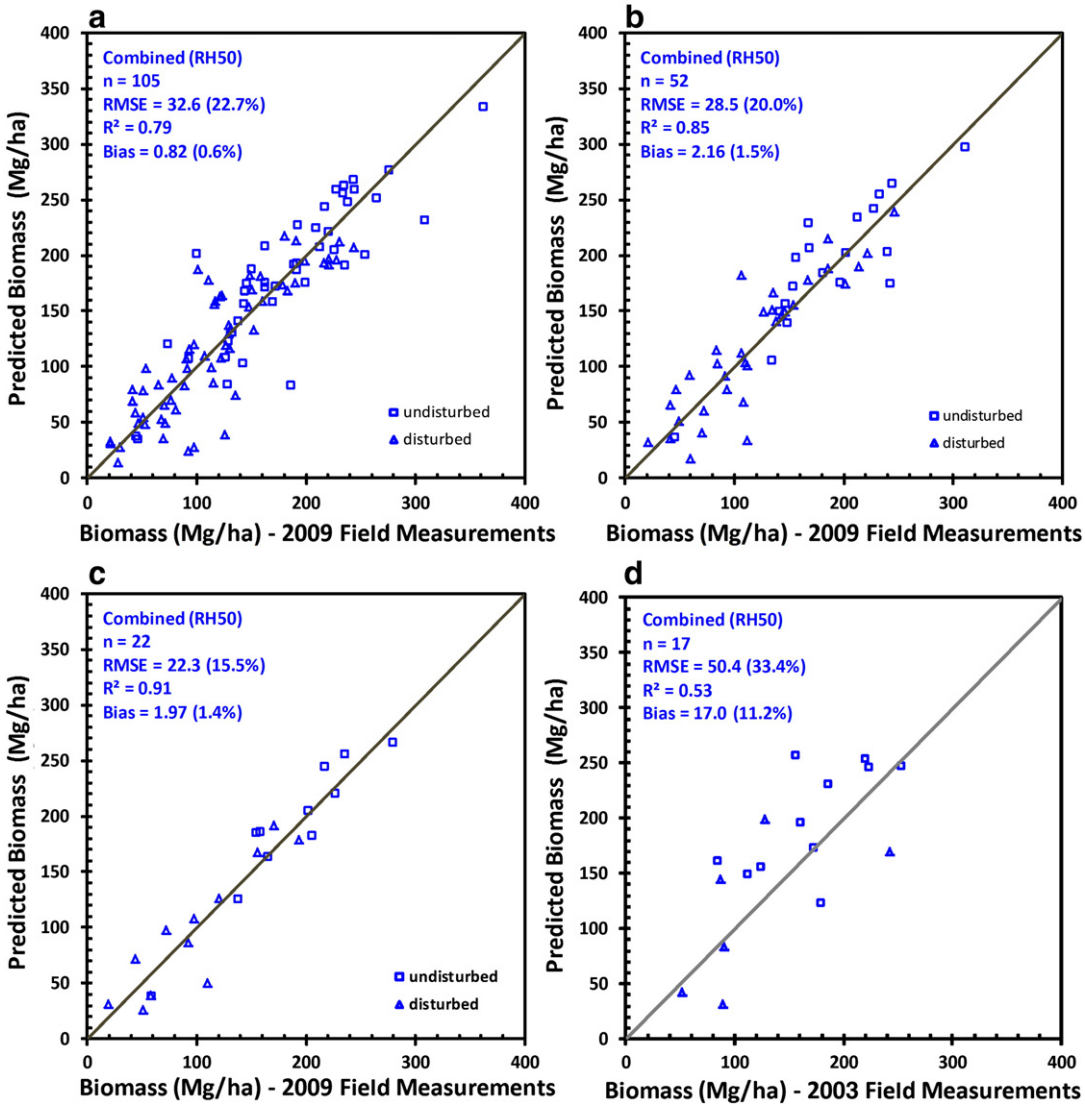

Fig. 8. Evaluation of combined footprint-level RH50 model in 2009, with the solid line for y = x. (a) 0.25 ha field plots; (b) 0.5 ha field plots; (c) 1.0 ha field plots in 2009; (d) ~0.5 ha field plots in 2003. All results were from the application of combined model. Rectangle dots represent the undisturbed points, and triangle dots represent the disturbed points.

4.3. Biomass mapping from LVIS data

The biomass maps (Fig. 10) from LVIS data for year 2003 and 2009 were produced using the RH50 regression model and were averaged to 1.0 ha spatial resolution. The biomass ranges up to 350 Mg·ha^{-1}. A color of orange (0–50 Mg·ha^{-1}) to dark green (>300 Mg·ha^{-1}) indicates an increase of biomass. Gray color represents the areas of no data and non-forest. The overall similar patterns of biomass can be seen from both years of 2003 and 2009. As shown in Fig. 10, the north-west region with biomass less than 100 Mg·ha^{-1} at HF site in 2009 was mostly caused by select-cut (i.e. shelter-wood harvest, removed large trees accounting for about 1/3 of the basal area) and

Table 5
Evaluation of the footprint-level disturbance-specific RH50 and RH75 models by plot-level field data in 2009 and 2003.

Model	Year	Plot-size	N	Mean of field (Mg·ha^{-1})	Mean of predict (Mg·ha^{-1})	R^2	RMSE (Mg·ha^{-1})	RMSE (%)	Bias (Mg·ha^{-1})	Bias (%)
RH50		**0.25 ha**	**105**	**143.6**	**140.6**	**0.78**	**34.7**	**24.2**	**−3.0**	**−2.1**
	2009	**0.5 ha**	**52**	**142.7**	**139.7**	**0.80**	**31.3**	**21.9**	**−2.9**	**−2.1**
		1.0 ha	**22**	**143.8**	**145.8**	**0.91**	**23.1**	**16.1**	**+0.9**	**+0.6**
	2003	**0.5 ha**	**17**	**151.0**	**170.9**	**0.51**	**54.6**	**36.2**	**+19.9**	**+13.2**
RH75		0.25 ha	105	143.6	142.0	0.73	37.8	26.3	−1.7	−1.2
	2009	0.5 ha	52	142.7	140.9	0.75	35.4	24.8	−1.9	−1.3
		1.0 ha	22	143.8	145.4	0.86	27.9	19.4	+1.6	+1.1
	2003	0.5 ha	17	151.0	171.3	0.48	57.4	38.0	+20.3	+13.4

N: number of sample; Mean of field: mean biomass averaged over samples at plot-level; Mean of predict: mean predicted biomass averaged over samples at plot-level; Bolded data are models with best performance at corresponding scale and year.

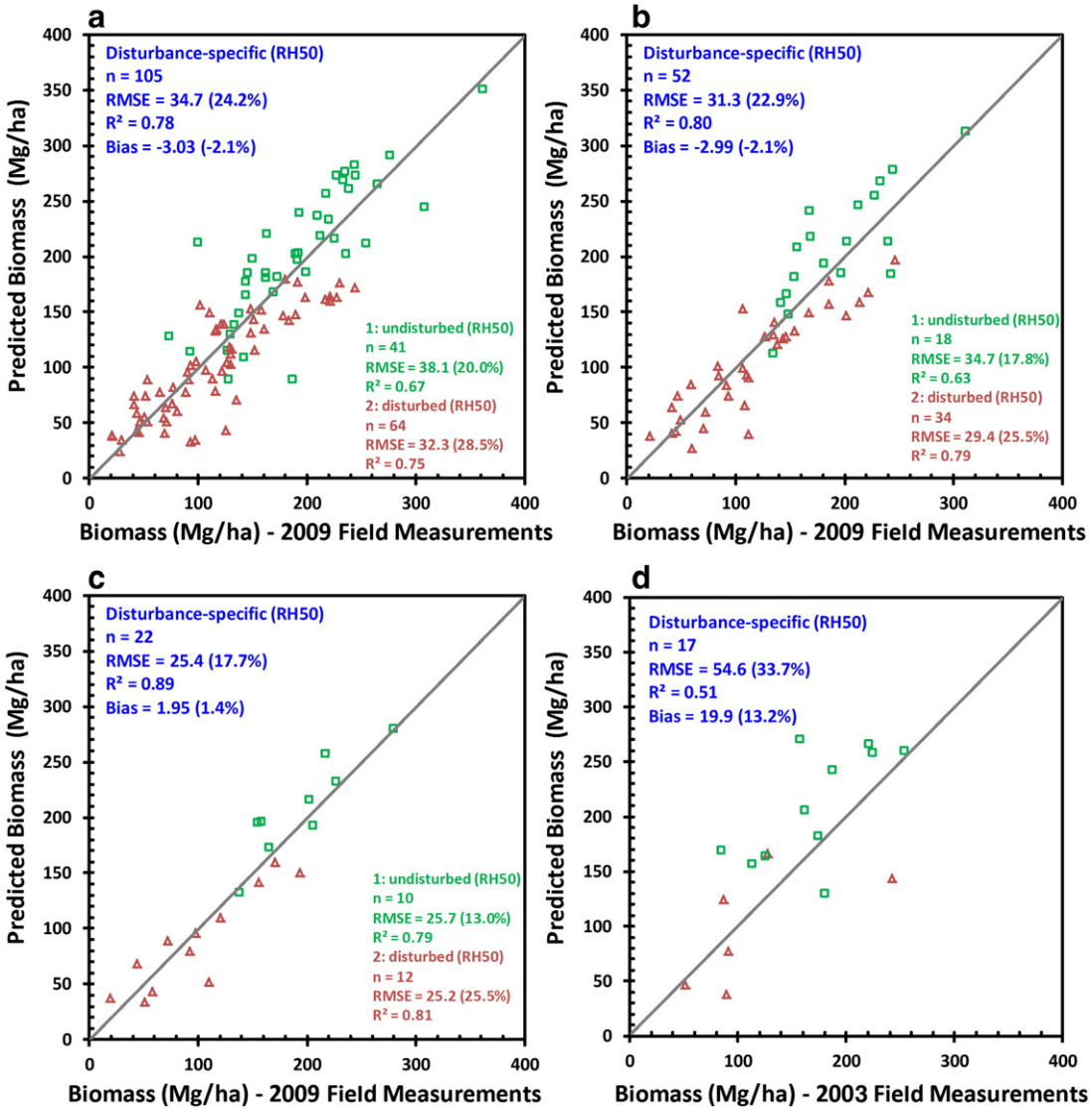

Fig. 9. Evaluations of disturbance-specific RH50 footprint-level biomass model, with solid line for y = x. (a) 0.25 ha field plots; (b) 0.5 ha field plots; (c) 1.0 ha field plots in 2009; (d) ~0.5 ha field plots in 2003. Different colors indicate the different models were used: rectangle dots (green) represent the undisturbed group, and triangle dots (red) represent the disturbed group.

stripe-cut (i.e. systematically removed stems in rows). The undisturbed forests in the center of the map (outlined by pink polygon in dotted line) were with high value of biomass (>300 Mg·ha^{-1}). For PEF in 2003 and 2009, high biomass regions were observed in the south and west region of the map. Low biomass regions with less than 50 Mg·ha^{-1} in the north-east were the woody wetland along the Penobscot River.

4.4. Biomass change mapping

Fig. 11(a) and (b) shows the changes of biomass (green to red color) from 2003 to 2009 at the two study sites, corresponding to the disturbance maps of Fig. 11(c), (d), and (e). It can be seen that most of the changes are consistent with the forest disturbance patterns detected by the LTSS-VCT product and the historical management map.

At HF site, biomass changes in the undisturbed near-mature forests (center of the map, highlighted by pink polygon in dotted line) were mostly positive (5 to 15 Mg·ha^{-1}) or near neutral (−5 to 5 Mg·ha^{-1}). The average annual biomass accumulation from undisturbed forest and regrowth is +4.4 Mg·ha^{-1}. The area surrounding this undisturbed forest shows strong negative change (in red, represent <−50 Mg·ha^{-1}). Most areas along the roads are the degraded forests from select-cut between 2003 and 2008 (filled irregular dots) as shown in Fig. 11(d). The average annual biomass reduction rate from forest disturbance is −7.0 Mg·ha^{-1}. Several patches highlighted with yellow in Fig. 11(c) show an increasing biomass during 2003 to 2009, due to the forest regrowth after clear-cut in the 1980s or stripe-cut in the 1990s. At PEF site, patches of strong negative biomass changes with red color in Fig. 11(c) were sparsely distributed over the study region. Most of them were detected by LTSS-VCT disturbance product in Fig. 11(e). The average annual biomass reduction rate from forest disturbance is −6.2 Mg·ha^{-1}. The woody wetlands with low biomass along the Penobscot River were regrowth from clear-cut prior to 2002. The average annual biomass accumulation from regrowth is +4.4 Mg·ha^{-1}.

5. Discussion

Our results highlight four important issues concerning biomass mapping from waveform LiDAR: (1) the feasibility of the prediction

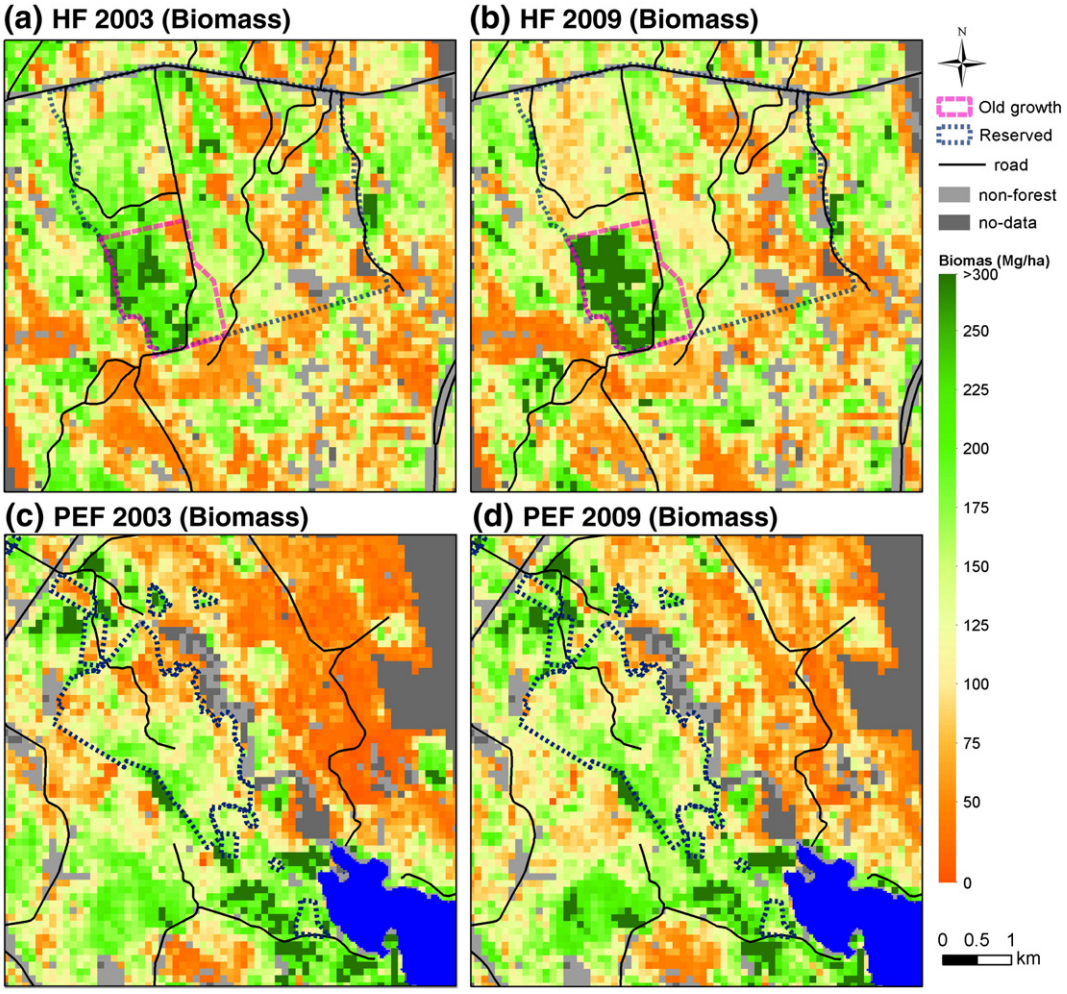

Fig. 10. Biomass map for HF site (a) and (b), and PEF site (c) and (d) in 2003 and 2009 at 1.0 ha level by the combined RH50 models. A color of orange to dark green indicates an increase of biomass. At HF site, pink polygon is near matured old-growth forest; and dark blue polygon is the outline of reserve area.

model at the LiDAR footprint, (2) the effect of forest disturbances on the biomass prediction model, (3) the effect of map scale and footprint density on the biomass estimation, and (4) the application of the footprint-level model for biomass change detection.

5.1. Prediction model at LiDAR footprint-level

The results in our study sites demonstrate that LiDAR footprint-level models could be developed and applied to mapping biomass, with 91% explanation of total variance, a RMSE of 22.4 $Mg \cdot ha^{-1}$ (15.6%) for the combined RH50 model at 1.0 ha plot-level. Two main factors lead to this conclusion. First, the accurate location provided by DGPS and high quality LVIS data reduced the geolocation errors. On the one hand, in our study, all footprint-level field measurements and sampling plots at HF in 2010 and 2011 and at PEF in 2009 were located using DGPS with a measurement error of 0.5–3.0 m (best case was 0.5–1.0 m). On the other hand, increased accuracy of the geolocation has been reported for the LVIS product released after 2003 by improved post data processing. Reprocessed 2003 LVIS data which using the same waveform analysis method are more consistent with 2009 LVIS data. Therefore geolocation errors are mostly avoided for the data used in the study. Secondly, the footprint size of LVIS facilitates the application of models at the footprint-level. LVIS data has a 20 m diameter footprint, which generally corresponds to the largest tree crowns, and thus can capture canopy characteristics (Dubayah et al., 2000).

5.2. Disturbance effect

Footprint-level regression models differed between undisturbed and disturbed forest, different species composition. Previous study (Anderson et al., 2006, 2008) has mentioned the effect of species composition to the biomass estimation. Forest disturbances change the spatial structure as well as the species composition. The statistical tests reveal a significant difference at 95% confidence level between models for the disturbed and undisturbed forests. The disturbance-specific models performed slightly better for biomass estimation than the combined model (Table 3). But the evaluation results (Tables 4 and 5) at different plot-levels from 0.25 ha, 0.5 ha to 1.0 ha showed almost the same biomass estimation accuracies for the combined and disturbance-specific models. The evaluation of biomass estimation shows that the combined RH50 model overpasses the combined RH75 model, and the disturbance-specific RH50 and RH75 models regardless of scale. These results weaken the importance of introducing disturbance factor into footprint-level model. It is reasonable for the effect of disturbance weaker at plot levels because averaging of LVIS footprints in plot will reduce the disturbance effect. The combined model was used for biomass mapping in this

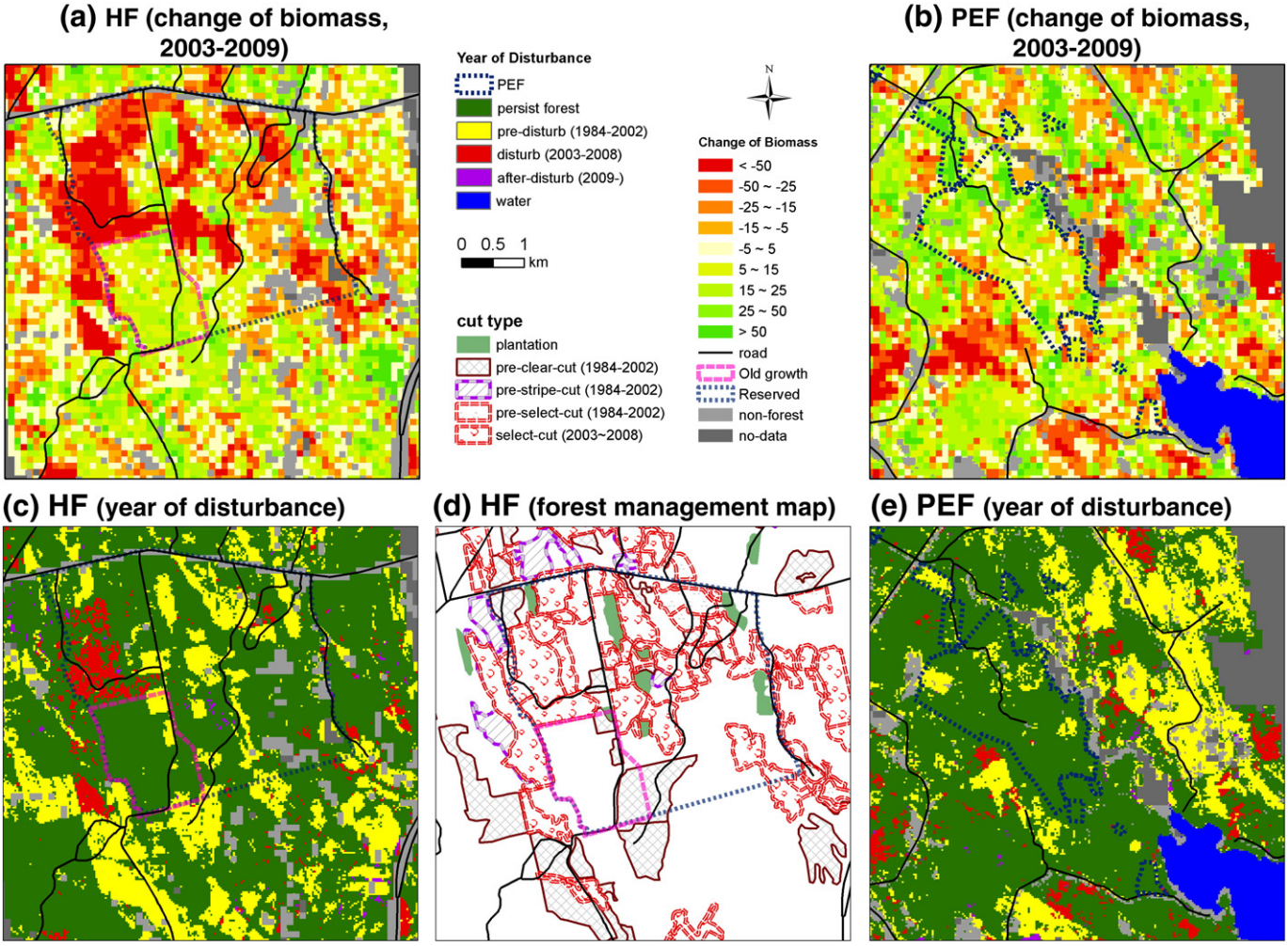

Fig. 11. Change of biomass for HF site (a) and PEF site (b) from 2003 to 2009 at 1.0 ha level by the combined RH50 models. (c) and (e) are the years of disturbances: disturbances prior to 2002 (yellow), between 2003 and 2008 (red), and after the 2009 (purple). (d) is the forest management map of HF created from information from private owner (international paper company) and Google images. The plantation is represented with green solid filled polygons. The clear-, select-, and stripe-cuts prior to 2002 are outlined with dark red solid lines with gray cross-hatched pattern, purple long dotted lines, and red double long dashed lines with gray stripes, respectively. The select-cut during 2003 to 2008 is outlined by red double dashed lines with irregular dots. At HF site, pink polygon is the near matured forest; and dark blue polygon is the outline of reserved area. The select-cut during 2003 to 2008 is outlined by red double dashed lines with irregular dots. At HF site, pink polygon is the near matured forest; and dark blue polygon is the outline of reserved area.

study. However, we still recommend considering the disturbance effect in area with more complicated species composition.

On the other hand, it is important to note the potential error that can be introduced by the classification of disturbance from LTSS-VCT. Based on field notes, recent Google Earth imagery and LTSS-VCT product, we are confident in the accurate classification of disturbance for our field samples. For a broader region more efforts are need to guarantee the accuracy in identification of disturbance. Careful application of a disturbance dataset is recommended when conducting forest biomass change assessments.

5.3. Map scale and footprint density

Biomass maps were produced by application of prediction models developed at the footprint-level (~0.03 ha; 20 m diameter circle plot) and re-sample the footprint biomass into map grids. The field biomass samples at different plot-levels (0.25 ha, 0.5 ha, and 1.0 ha; rectangular plot) served as independent data for evaluation of the accuracies of biomass maps.

Fig. 12 shows the RMSE (%) of the biomass prediction models developed at footprint level, and the evaluations at 0.25 ha, 0.5 ha and 1.0 ha plot-levels. We can see a decreasing trend for RMSE (%) with increasing size of plots. At 1.0 ha plot, the RMSE (%) from disturbance-specific and combined models is similar and is much lower than at other smaller plot levels. Recent studies (Mascaro et al., 2011; Frazer et al., 2011) have indicated that 1.0 ha plots could capture biomass with low and stable errors close to 10%. Therefore, we used a 1.0 ha scale for the biomass mapping and change detection using the combined RH50 models.

Fig. 13 shows the sensitivity of (a) RMSE (%) and (b) R^2 to the footprint density (pt/ha) from 0.25 ha, 0.5 ha and 1.0 ha plot-levels. With the increasing of footprint density, there is a decreasing trend for RMSE (%), and an increasing trend of R^2 at 0.25 ha, 0.5 ha and 1.0 ha plot-levels. At all three plot-levels, a critical inflection point where point density equals 16 pt/ha was observed regardless of scale. The relationship between RMSE (%) and point density becomes stable after reaching this inflection point. This is the same to the trend of R^2. Therefore, optimal point density of 16 is suggested for a high quality of biomass estimation at 1.0 ha plot-level. This is feasible because the average footprint density within our field sampled plots was over 50 pt/ha with a 20 m nominal spacing both along and across track.

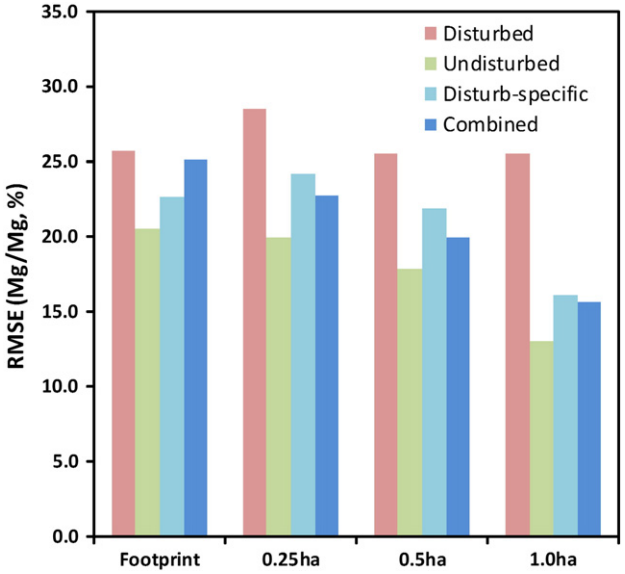

Fig. 12. RMSE (%) of the RH50 biomass prediction models developed at footprint-level and the evaluations at 0.25, 0.5 and 1.0 ha scales. Bars from left to right represent best models for disturbed (pink), undisturbed (green), disturbance-specific (light blue), and combined (dark blue).

5.4. Application of footprint-level model for biomass change mapping

The footprint-level models were developed using 2009 data in this study and then applied to both 2009 and 2003 data for mapping forest biomass and its change. Repeat acquisition of LiDAR data has been used for detecting changes of canopy height and biomass. Dubayah et al. (2010) recommended using the relationship between the biomass change and change in LVIS-derived range-based forest canopy height metrics for biomass change studies to avoid using two sets of biomass estimation models. However, due to limited co-incident field measurements at either footprint or plot level, we couldn't develop the similar equations. Instead, footprint-level plots were selected to develop a uniform biomass equation and then this equation was applied to LVIS data in both 2003 and 2009. In addition to the forest spatial structural variations from disturbances, other factors such as species composition, seasonal changes of leaf area index, reflectance of ground surface, etc. will also affect the LiDAR waveform metrics and the biomass prediction model. This should be considered in applying prediction model developed at a place at certain time to other places or data acquired at different seasons. The LiDAR waveform data used in this study were acquired using the same instrument (LVIS) and at the same season (August) in 2003 and 2009. The processing of the LVIS data is also the same for 2003 and 2009 data. Therefore the common relationship between biomass and LiDAR waveform metrics should keep consistent from 2003 to 2009.

6. Conclusion

Estimating biomass dynamics over relatively short time scales is a difficult task, yet is central to obtaining a better understanding of the effects of disturbance and subsequent regrowth on the terrestrial carbon cycle. There is additionally a strong and growing need to develop effective mapping and monitoring in support of climate treaty frameworks such as REDD+ (Goetz & Dubayah, 2011). Our work presented here is one example of a remote sensing approach to this problem.

Our ability to quantify changes with LiDAR remote sensing in particular is based on having sufficient ground data with adequate geolocation from which to develop predictive models. Ground data sets that consistently monitor change at the same plots are rare; indeed our study lacked these, and this should be a priority for the terrestrial ecology community moving forward. Change studies are also dependent on having sufficient LiDAR coverage to develop spatially meaningful maps. Ideally such coverage would be wall-to-wall, but practically that may not be achievable nor may it be entirely necessary. Our errors were minimized when footprint coverage approached about 50% of the area of 1.0 ha plots (16 footprints) with no improvement beyond that. This is a particularly important point when considering monitoring from space-based LiDAR, which is unlikely to have swath-mapping capability in the near term.

While our experiment showed improvement in biomass prediction when disturbance was included, the results were not compelling. We doubt that this conclusion is generalizable beyond the present study. While canopy metrics must implicitly include the effects of disturbance as reflected in height, other factors also control height, most notably climate and edaphic factors. Thus more work is needed to untangle the relationships between these factors, disturbance, and their manifestation in height metrics. That said, the fusion of Landsat disturbance products with time series of LiDAR data is a powerful approach to quantifying landscape level changes in vegetation structure and will certainly be exploited with increasing frequency in future studies.

Ultimately, there is distance to travel before we can confidently monitor biomass and canopy structure dynamics at policy-relevant scales with the requisite accuracy in a consistent and transparent framework from remote sensing. LiDAR remote sensing is so new that only now are we able to evaluate data sets with sufficient time intervals between them, and for which contemporaneous field estimates are available. We anticipate that as more investigations undertake such studies, rapid progress will result in this important capability.

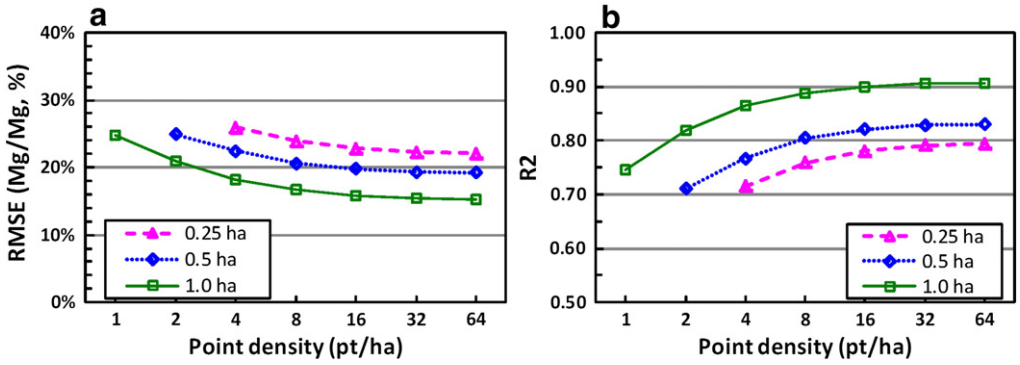

Fig. 13. Sensitivity of RMSE% (a) and R^2 (b) to the density of footprints within the plot (pt/ha) at 0.25 ha, 0.50 ha and 1.0 ha plot-levels; RMSE (%) and R^2 values were from the combined RH50 footprint-level biomass prediction model.

Acknowledgments

This work was done with financial support from the NASA Terrestrial Ecology Program (no. NNX09AG66G). LiDAR datasets were provided by the LVIS team in the Laser Remote Sensing Branch at NASA GSFC with supports from University of Maryland (UMD), College Park. Field data were collected by teams from NASA GSFC, JPL, UMD, and University of Maine in October 2003, August 2009 to 2011 funded by NASA. The authors would like to thank Prof. John Lee for collection of forest management maps and assistance in field measurements, and Prof. Chengquan Huang for acquisition and processing of LTSS-VCT disturbance product over the study area.

References

Anderson, J., Martin, M. E., Smith, M. L., Dubayah, R. O., Hofton, M. A., Hyde, P., et al. (2006). The use of waveform LiDAR to measure northern temperate mixed conifer and deciduous forest structure in New Hampshire. *Remote Sensing of Environment*, *105*, 248–261.

Anderson, J. E., Plourde, L. C., Martin, M. E., Braswell, B. H., Smith, M. -L., Dubayah, R. O., et al. (2008). Integrating waveform lidar with hyperspectral imagery for inventory of a northern temperate forest. *Remote Sensing of Environment*, *112*, 1856–1870.

Asner, G. P., Hughes, R. F., Mascaro, J., Uowolo, A. L., Knapp, D. E., Jacobson, J., et al. (2011). High-resolution carbon mapping on the million-hectare Island of Hawaii. *Frontiers in Ecology and the Environment*, *9*, 434–439.

Asner, G. P., Mascaro, J., Muller-Landau, H. C., Vieilledent, G., Vaudry, R., Rasamoelina, M., et al. (2012). A universal airborne LiDAR approach for tropical forest carbon mapping. *Oecologia*, *1–14*.

Asner, G. P., Powell, G. V. N., Mascaro, J., Knapp, D. E., Clark, J. K., Jacobson, J., et al. (2010). High-resolution forest carbon stocks and emissions in the Amazon. *Proceedings of the National Academy of Sciences*, *107*, 16738–16742.

Bergen, K. M., Goetz, S. J., Dubayah, R. O., Henebry, G. M., Hunsaker, C. T., Imhoff, M. L., et al. (2009). Remote sensing of vegetation 3-D structure for biodiversity and habitat: Review and implications for lidar and radar spaceborne missions. *Journal of Geophysical Research*, *114*, G00E06.

Blair, J. B., Hofton, M. A., & Rabine, D. L. (2006). *Processing of NASA LVIS elevation and canopy (LGE, LCE and LGW) data products, version 1.02.* Greenbelt, Md.: NASA Goddard Space Flight Cent (Available at http://lvis.gsfc.nasa.gov).

Blair, J. B., Rabine, D. L., & Hofton, M. A. (1999). The Laser Vegetation Imaging Sensor: A medium-altitude, digitisation-only, airborne laser altimeter for mapping vegetation and topography. *ISPRS Journal of Photogrammetry and Remote Sensing*, *54*, 115–122.

Chazdon, R. L. (2003). Tropical forest recovery: Legacies of human impact and natural disturbances. *Perspectives in Plant Ecology, Evolution and Systematics*, *6*, 51–71.

Clark, D. B., & Kellner, J. R. (2012). Tropical forest biomass estimation and the fallacy of misplaced concreteness. *Journal of Vegetation Science*, *23*, 1191–1196.

Drake, J. B., Dubayah, R. O., Clark, D. B., Knox, R. G., Blair, J. B., Hofton, M. A., et al. (2002). Estimation of tropical forest structural characteristics using large-footprint LiDAR. *Remote Sensing of Environment*, *79*, 305–319.

Drake, J. B., Knox, R. G., Dubayah, R. O., Clark, D. B., Condit, R., Blair, J. B., et al. (2003). Above-ground biomass estimation in closed canopy Neotropical forests using lidar remote sensing: Factors affecting the generality of relationships. *Global ecology and biogeography* (pp. 147–159): Wiley-Blackwell.

Dubayah, R. O., Knox, R. G., Hofton, M. A., Blair, J. B., & Drake, J. B. (2000). In M. J. Hill, & R. Aspinall (Eds.), *Land surface characterization using lidar remote sensing* (pp. 25–38). Singapore: International Publisher Direct.

Dubayah, R. O., Sheldon, S. L., Clark, D. B., Hofton, M. A., Blair, J. B., Hurtt, G. C., et al. (2010). Estimation of tropical forest height and biomass dynamics using lidar remote sensing at La Selva, Costa Rica. *Journal of Geophysical Research*, *115*, G00E09.

Frazer, G. W., Magnussen, S., Wulder, M. A., & Niemann, K. O. (2011). Simulated impact of sample plot size and co-registration error on the accuracy and uncertainty of LiDAR-derived estimates of forest stand biomass. *Remote Sensing of Environment*, *115*, 636–649.

Goetz, S., & Dubayah, R. (2011). Advances in remote sensing technology and implications for measuring and monitoring forest carbon stocks and change. *Carbon Management*, *2*, 231–244.

Gonzalez, P., Asner, G. P., Battles, J. J., Lefsky, M. A., Waring, K. M., & Palace, M. (2010). Forest carbon densities and uncertainties from LiDAR, QuickBird, and field measurements in California. *Remote Sensing of Environment*, *114*, 1561–1575.

Hall, F. G., Bergen, K., Blair, J. B., Dubayah, R., Houghton, R., Hurtt, G., et al. (2011). Characterizing 3D vegetation structure from space: Mission requirements. *Remote Sensing of Environment*, *115*, 2753–2775.

Hollinger, D. Y., Goltz, S. M., Davidson, E. A., Lee, J. T., Tu, K., & Valentine, H. T. (1999). Seasonal patterns and environmental control of carbon dioxide and water vapour exchange in an ecotonal boreal forest. *Global Change Biology*, *5*, 891–902.

Huang, C., Goward, S. N., Masek, J. G., Thomas, N., Zhu, Z., & Vogelmann, J. E. (2010). An automated approach for reconstructing recent forest disturbance history using dense Landsat time series stacks. *Remote Sensing of Environment*, *114*, 183–198.

Hyde, P., Dubayah, R., Peterson, B., Blair, J. B., Hofton, M., Hunsaker, C., et al. (2005). Mapping forest structure for wildlife habitat analysis using waveform lidar: Validation of montane ecosystems. *Remote Sensing of Environment*, *96*, 427–437.

Jenkins, J. C., Chojnacky, D. C., Heath, L. S., & Birdsey, R. A. (2003). National-scale biomass estimators for United States tree species. *Forest Science*, *49*, 12–35.

Jenkins, J. C., Chojnacky, D. C., Heath, L. S., & Birdsey, R. A. (2004). Comprehensive database of diameter-based biomass regressions for North American tree species. *General technical report NE-319*. Newtown Square, PA: U.S. Department of Agriculture, Forest Service, Northeastern Research Station.

Kellndorfer, J. M., Walker, W. S., LaPoint, E., Kirsch, K., Bishop, J., & Fiske, G. (2010). Statistical fusion of lidar, InSAR, and optical remote sensing data for forest stand height characterization: A regional-scale method based on LVIS, SRTM, Landsat ETM+, and ancillary data sets. *Journal of Geophysical Research*, *115*, G00E08.

Lefsky, M. A. (2010). A global forest canopy height map from the Moderate Resolution Imaging Spectroradiometer and the Geoscience Laser Altimeter System. *Geophysical Research Letters*, *37*, L15401.

Lefsky, M. A., Cohen, W. B., Harding, D. J., Parker, G. G., Acker, S. A., & Gower, S. T. (2002). Lidar remote sensing of above ground biomass in three biomes. *Global Ecology and Biogeography*, *11*, 393–399.

Lefsky, M. A., Harding, D., Cohen, W. B., Parker, G., & Shugart, H. H. (1999). Surface lidar remote sensing of basal area and biomass in deciduous forests of Eastern Maryland, USA. *Remote Sensing of Environment*, *67*, 83–98.

Lefsky, M. A., Hudak, A. T., Cohen, W. B., & Acker, S. A. (2005a). Geographic variability in lidar predictions of forest stand structure in the Pacific Northwest. *Remote Sensing of Environment*, *95*, 532–548.

Lefsky, M. A., Keller, M., Pang, Y., De Camargo, P. B., & Hunter, M. O. (2007). Revised method for forest canopy height estimation from Geoscience Laser Altimeter System waveforms. *Journal of Applied Remote Sensing*, *1*, 013537.

Lefsky, M. A., Turner, D. P., Guzy, M., & Cohen, W. B. (2005b). Combining LiDAR estimates of aboveground biomass and Landsat estimates of stand age for spatially extensive validation of modeled forest productivity. *Remote Sensing of Environment*, *95*, 549–558.

Lim, K. S., & Treitz, P. M. (2004). Estimation of above ground forest biomass from airborne discrete return laser scanner data using canopy-based quantile estimators. *Scandinavian Journal of Forest Research*, *19*, 558–570.

Lu, D. (2006). The potential and challenge of remote sensing-based biomass estimation. *International Journal of Remote Sensing*, *27*, 1297–1328.

Mallet, C., & Bretar, F. (2009). Full-waveform topographic lidar: State-of-the-art. *ISPRS Journal of Photogrammetry and Remote Sensing*, *64*, 1–16.

Mascaro, J., Detto, M., Asner, G. P., & Muller-Landau, H. C. (2011). Evaluating uncertainty in mapping forest carbon with airborne Lidar. *Remote Sensing of Environment*, *115*, 3770–3774.

Mather, P. M. (2004). *Computer processing of remotely sensed images.* Chichester, West Sussex, England: John Wiley & Sons Ltd.

Means, J. E., Acker, S. A., Harding, D. J., Blair, J. B., Lefsky, M. A., Cohen, W. B., et al. (1999). Use of large-footprint scanning airborne LiDAR to estimate forest stand characteristics in the western cascades of Oregon. *Remote Sensing of Environment*, *67*, 298–308.

Næsset, E., & Gobakken, T. (2008). Estimation of above- and below-ground biomass across regions of the boreal forest zone using airborne laser. *Remote Sensing of Environment*, *112*, 3079–3090.

Nelson, R., Ranson, K. J., Sun, G., Kimes, D. S., Kharuk, V., & Montesano, P. (2009). Estimating Siberian timber volume using MODIS and ICESat/GLAS. *Remote Sensing of Environment*, *113*, 691–701.

Nilsson, M. (1996). Estimation of tree heights and stand volume using an airborne lidar system. *Remote Sensing of Environment*, *56*, 1–7.

Ni-Meister, W., Lee, S., Strahler, A. H., Woodcock, C. E., Schaaf, C., Yao, T., et al. (2010). Assessing general relationships between aboveground biomass and vegetation structure parameters for improved carbon estimate from LiDAR remote sensing. *Journal of Geophysical Research*, *115*, G00E11.

Pang, Y., Zhao, F., Li, Z., Zhou, S., Deng, G., Liu, Q., et al. (2008). Forest height inversion using airborne LiDAR technology. *Journal of Remote Sensing*, *12*(1), 152–158 (in Chinese).

Ranson, K. J., & Sun, G. (2010). Effects of forest disturbances on forest structural parameters retrieval from lidar waveform data. *2010 IEEE International Geoscience and Remote Sensing Symposium (IGARSS)* (pp. 4370–4373).

Saatchi, S. S., Harris, N. L., Brown, S., Lefsky, M., Mitchard, E. T. A., Salas, W., et al. (2011). Benchmark map of forest carbon stocks in tropical regions across three continents. *Proceedings of the National Academy of Sciences*, *108*, 9899–9904.

Safford, L. O., Frank, R. M., & Little, E. L. (1969). *Trees and shrubs of the Penobscot experimental forest.* Penobscot County, Maine: Northeastern Forest Experiment Station.

Solberg, S., Astrup, R., Gobakken, T., Næsset, E., & Weydahl, D. J. (2010). Estimating spruce and pine biomass with interferometric X-band SAR. *Remote Sensing of Environment*, *114*, 2353–2360.

Sun, G., Ranson, K. J., Guo, Z., Zhang, Z., Montesano, P., & Kimes, D. (2011). Forest biomass mapping from LiDAR and radar synergies. *Remote Sensing of Environment*, *115*, 2906–2916.

Sun, G., Ranson, K. J., Kimes, D. S., Blair, J. B., & Kovacs, K. (2008). Forest vertical structure from GLAS: An evaluation using LVIS and SRTM data. *Remote Sensing of Environment*, *112*, 107–117.

Swatantran, A., Dubayah, R., Roberts, D., Hofton, M., & Blair, J. B. (2011). Mapping biomass and stress in the Sierra Nevada using LiDAR and hyperspectral data fusion. *Remote Sensing of Environment*, *115*, 2917–2930.

Thomas, N. E., Huang, C., Goward, S. N., Powell, S., Rishmawi, K., Schleeweis, K., et al. (2011). Validation of North American Forest Disturbance dynamics derived from Landsat time series stacks. *Remote Sensing of Environment*, *115*, 19–32.

Zhao, K., Popescu, S., Meng, X., Pang, Y., & Agca, M. (2011). Characterizing forest canopy structure with LiDAR composite metrics and machine learning. *Remote Sensing of Environment*, *115*, 1978–1996.